Monthly Notices
of the
ROYAL ASTRONOMICAL SOCIETY

MNRAS **453,** L16–L20 (2015) doi:10.1093/mnrasl/slv091

The extreme ultraviolet spectrum of the kinetically dominated quasar 3C 270.1

Brian Punsly[1]†★ and Paola Marziani[2]

[1]*ICRANet, Piazza della Repubblica 10, I-65100 Pescara, Italy*
[2]*INAF, Osservatorio Astronomico di Padova, I-35122 Padova, Italy*

Accepted 2015 July 5. Received 2015 July 3; in original form 2015 May 6

ABSTRACT

Only a handful of quasars have been identified as kinetically dominated, their long-term time-averaged jet power, $\overline{Q}$, exceeds the bolometric thermal emission, $L_{\rm bol}$, associated with the accretion flow. This Letter presents the first extreme ultraviolet (EUV) spectrum of a kinetically dominated quasar, 3C 270.1. The EUV continuum flux density of 3C 270.1 is very steep, $F_\nu \sim \nu^{-\alpha_{\rm EUV}}$, $\alpha_{\rm EUV} = 2.98 \pm 0.15$. This value is consistent with the correlation of $\overline{Q}/L_{\rm bol}$ and $\alpha_{\rm EUV}$ found in previous studies of the EUV continuum of quasars, the EUV deficit of radio loud quasars. Curiously, although ultraviolet broad absorption line (BAL) troughs in quasar spectra are anticorrelated with $\overline{Q}$, 3C 270.1 has been considered a BAL quasar based on an SDSS spectrum. This claim is examined in terms of the EUV spectrum of O VI and the highest resolution C IV spectrum in the archival data and the SDSS spectrum. First, from [O III]4959,5007 (IR) observations and the UV spectral lines, it is concluded that the correct redshift for 3C 270.1 is 1.5266. It is then found that the standard measure of broad absorption, BALnicity = 0, for Mg II 2800, C IV 1549 and O VI 1032 in all epochs.

Key words: accretion, accretion discs – Black hole physics – MHD – galaxies: active – galaxies: jets.

1 INTRODUCTION

The quasar 3C 270.1 contains one of the most powerful jets of any known active galactic nucleus. The jet power greatly exceeds any other associated with a quasar that has been claimed to have an ultraviolet (UV) broad absorption line (BAL). These extreme properties of 3C 270.1 offer a unique laboratory for exploring the mechanism of relativistic jet formation. The long-term time averaged jet power, $\overline{Q}$, determined from low-frequency radio lobe emission, is so extreme that the quasar was classified as kinetically dominated $\overline{Q}/L_{\rm bol} > 1$, where $L_{\rm bol}$ is the bolometric thermal emission associated with the accretion flow (Punsly 2007). The physical relevance of this result is uncertain since the plasma in the radio lobes was ejected from the central engine $>10^5$ years before the UV emitting gas reached the environs of the central black hole. This Letter uses the EUV spectrum of 3C 270.1 to address two fundamental issues. First, can a quasar actually emit more power in the jet than is being radiated as thermal emission? Secondly, why are BAL winds anticorrelated with jet emission on supergalactic scales? Both of the issues provide valuable clues to the jet launching mechanism.

★E-mail: brian.punsly1@verizon.net
†Permanent address: 1415 Granvia Altamira, Palos Verdes Estates, 90274 CA, USA.

Even though the radio lobes of powerful radio-loud quasars (RLQs) are located light travel times typically 10^5–10^6 yr from the central black hole, they tend to be connected by a radio jet. Quasars with radio lobes on supergalactic scales are very rare, ∼1.7 per cent of all quasars have such extended structure (deVries, Becker & White 2006). The existence of the connective bridge formed by the jet implies that the energy source seems persistent for long periods of time. It is a mystery how the jet can be powered for so long and it is unclear how much the jet power fluctuates over 10^6 yr compared to its average value. In Punsly (2014, 2015), it was shown that $\overline{Q}/L_{\rm bol}$ (which depends on a long term average) was correlated with the deficit of EUV emission quantified by $\alpha_{\rm EUV}$ (the flux density scales as $F_\nu \propto \nu^{-\alpha_{\rm EUV}}$). The EUV is believed to be the putative Wien tail of the optically thick emission from the innermost region of the accretion flow; a region of the flow that interacts in real time with the central black hole (Punsly 2015). Like the bridge formed by the jet, this also seems to indicate a rather persistent dynamic near the central black hole that is sustained for most of $\sim 10^6$ yr of the radio source lifetime. Furthermore, there is only a modest degree of scatter from the average trend in the $\overline{Q}/L_{\rm bol} - \alpha_{\rm EUV}$ plane (see Fig. 2) for the RLQ population. The scatter plot samples quasars at random epochs in their radio loud lifetime. This modest scatter indicates that the fluctuations in the dynamics are typically not that large. Some 'baseline' dynamical configuration seems to exist in each quasar more often than not for the majority of these objects. In

the next section, this is interpreted with other evidence to indicate that 3C 270.1 had a powerful jet, $Q(t)/L_{\rm bol} \sim 1$, when the EUV radiation was emitted.

Another aspect of this study is to analyse the claim of Gibson et al. (2009) that 3C 270.1 has broad absorption in C IV and not associated absorption. This conclusion contradicts previous findings (Anderson et al. 1987). This is physically significant since there are only a handful of known RLQs with extended structure on supergalactic scales that are bona fide BALQSOs as defined by the BALnicty index. None of these have $\overline{Q}/L_{\rm bol}$ within a factor of 10 of 3C 270.1. This conflict is analysed in Section 3. Quantifying the jet power and the interplay between the BAL wind suppression and jet power provides fundamental insight into the nature of the jet launching in quasars.

2 THE EUV SPECTRUM AND JET POWER

3C 270.1 was observed on 2000 July 24 for 2380 s with the *Hubble Space Telescope* (*HST*) with the Space Telescope imaging spectrograph and G230L grating. The data were downloaded from Mikulski Archive the for Space Telescope and corrected for Galactic extinction with the Cardelli Clayton and Mathis absorption law (Cardelli, Clayton & Mathis 1989). The absorption from the Ly α valley was de-convolved from the data using the empirical statistical methods of Zheng et al. (1997). An intervening Lyman-limit system near the quasar systemic redshift was removed with the decrement method (Shull, Stevans & Danforth 2012; Punsly 2014). Namely, the Lyman-limit system was removed by assuming a single cloud with a ν^{-3} opacity and an absorption that was scaled by the decrement between the continuum and the trough depth. This was considered acceptable because the power law above the Lyman-limit system continues smoothly through the corrected region (see Fig. 1). The power law between 1100 and 700 Å is defined by $\alpha_{\rm EUV} = 2.98 \pm 0.15$. The top frame of Fig. 1 is the power-law fit (solid black line) to the continuum. The bottom frame is a fourth-order polynomial fit (solid red line) that provides an upper limit to the continuum in the analysis of O VI absorption in the next section.

A method that allows one to convert 151 MHz flux densities, F_{151} (measured in Jy), into estimates of long-term time-averaged jet power, $\overline{Q}$, (measured in erg s^{-1}) is given by equation (1) (Willott et al. 1999; Punsly 2005):

$$\overline{Q} \approx [(\boldsymbol{f}/15)^{3/2}]1.1 \times 10^{45} \left[X^{1+\alpha} Z^2 F_{151}\right]^{0.857} \ {\rm erg\,s^{-1}}, \quad (1)$$

$$Z \equiv 3.31 - (3.65) \times \left[X^4 - 0.203X^3 + 0.749X^2 + 0.444X + 0.205\right]^{-0.125}, \quad (2)$$

where $X \equiv 1 + z$, F_{151} is the total optically thin flux density from the lobes. Deviations from the overly simplified minimum energy estimates are combined into a multiplicative factor, $\boldsymbol{f}$, that represents the small departures from minimum energy, geometric effects, filling factors, protonic contributions and low-frequency cutoff (Willott et al. 1999). In Blundell & Rawlings (2000), it was argued that $10 < \boldsymbol{f} < 20$. Alternatively, there is another isotropic estimator in which the lobe energy is primarily inertial in form (Punsly 2005):

$$\overline{Q} \approx 5.7 \times 10^{44}(1+z)^{1+\alpha} Z^2 F_{151} \ {\rm erg\,s^{-1}}. \quad (3)$$

Define the radio spectral index, α, as $F_\nu \propto \nu^{-\alpha}$. Equation (1) with $\boldsymbol{f} = 20$ is the maximum upper bound on $\overline{Q}$ and equation (2) is the lower bound $\overline{Q}$ that is used in the following. In this Letter, we adopt the following cosmological parameters:

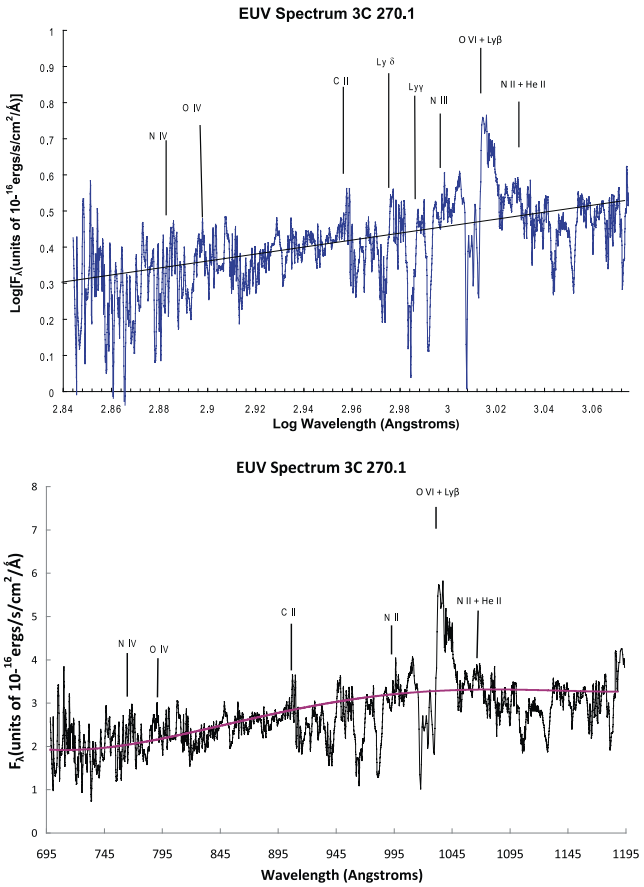

Figure 1. The EUV spectrum of 3C 270.1. The top frame is the power-law fit (solid black line) to the continuum. The bottom frame is a fourth-order polynomial fit (solid red line) to the continuum.

$H_0 = 70\,{\rm km\,s^{-1}\ Mpc^{-1}}$, $\Omega_\Lambda = 0.7$ and $\Omega_{\rm m} = 0.3$. The radio images in Garrington, Conway & Leahy (1991) indicate that this is a lobe-dominated quasar. Therefore, one expects the 151 MHZ flux density (14.96 Jy from the NASA Extragalatic Database) to be dominated by the radio lobe emission. Thus, from equations (1)–(3) that $\overline{Q} = 7.5 \times 10^{46} \pm 1.5 \times 10^{46}$ erg s^{-1}.

Since the data used here cover the peak of the Spectral Energy Distribution (SED) at $\lambda \approx 1100$ Å, an accurate expression, $L_{\rm bol} \approx 3.8\lambda L_\lambda(\lambda = 1100\,{\rm Å})$, can be used to estimate the accretion disc luminosity. This does not include reprocessed IR emission in distant molecular clouds (Davis & Laor 2011; Punsly 2014). From the flux density in Fig. 1, $L_{\rm bol} = 5.2 \times 10^{46} \pm 0.5 \times 10^{46}$ erg s^{-1}. Combining this with the estimate of $\overline{Q}$, above, $\overline{Q}/L_{\rm bol} = 1.4$. 3C 270.1 is kinetically dominated in this context.

The top frame of Fig. 2 places 3C 270.1 on the same scatter plot of $\log[\overline{Q}/L_{\rm bol}]$ and $\alpha_{\rm EUV}$ as the other quasars for which a similar data reduction was performed in Fig. 3 of Punsly (2015). 3C 270.1 has the most powerful jet and it lies at the end of the extrapolated trend of the other powerful RLQs. Fig. 2 relates real-time properties (meaning concurrent with the epoch that the data were sampled in the quasar rest frame), $L_{\rm bol}$ and $\alpha_{\rm EUV}$, with a long-term time-average property, $\overline{Q}$. The coefficient of determination to a linear fit is 0.5927 so the scatter is modest. Each data point in Fig. 2 is a random snapshot in time of the properties of the inner most accretion flow during the lifetime each RLQ. The degree of scatter indicates that there is a baseline or fiducial configuration of the central engine in each RLQ and the fluctuations over time

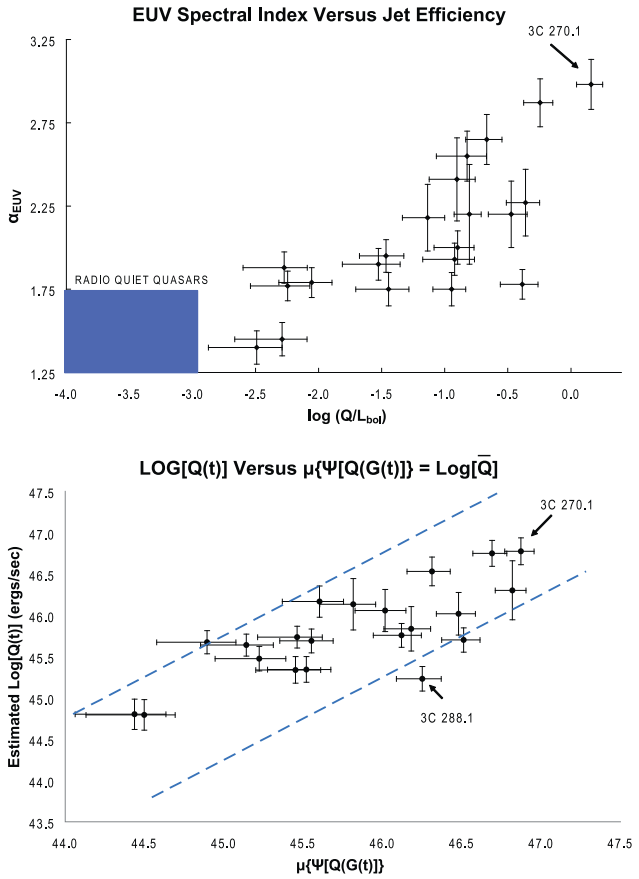

Figure 2. The top frame is a scatter plot of $\overline{Q}/L_{\rm bol}$ versus $\alpha_{\rm EUV}$. The bottom frame is a scatter plot of $Q(t)$ estimated from equation (6) relative to the 90 per cent confidence contours (blue dashed) of the probability distribution, $\Psi\{Q[G(t)]\}$, in equation (7).

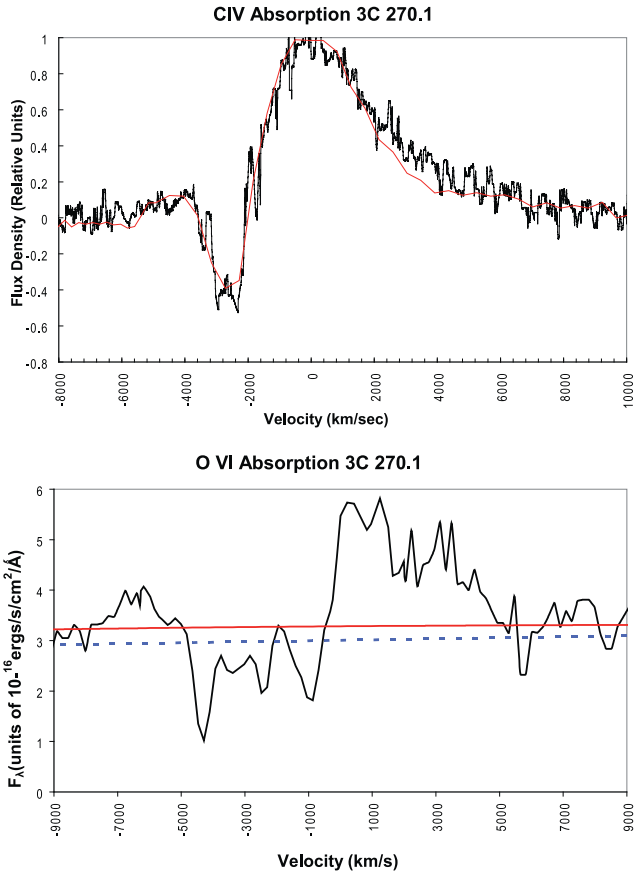

Figure 3. Ultraviolet absorption lines occur in the spectrum. The C IV line as measured by MMT is plotted in black in the top frame. The SDSS low-resolution C IV spectrum is overlaid in red. The data were referenced to the estimated continuum level. The O VI absorption and emission line is plotted in the bottom frame. The solid red line is the fourth order polynomial fit and the dashed blue line is the power-law fit to the continuum.

from this configuration are usually 'modest' and large fluctuations are not typical. This concept is quantified below in order to see if there is predictive power of real-time jet parameters from the data in Fig. 2. To begin with, segregate the real-time variables from $\overline{Q}$ by inverting the linear fit to the data in the top frame of Fig. 2. This process yields a real-time variable

$$G(t) = 2.58\alpha_{\rm EUV}(t) + \log\,[3.8\lambda L_\lambda(\lambda = 1100\,\text{Å})(t)/10^{45}\ \text{ergs/s}]. \quad (4)$$

As an alternative to a scatter plot in the $\log[\overline{Q}/L_{\rm bol}]$–$\alpha_{\rm EUV}$ plane (the top frame of Fig. 2), one can also consider the data scatter in the $\log[\overline{Q}]$–$G(t)$ plane. Define $\overline{\Psi}$ as the best-fitting power-law estimator of $\log(\overline{Q})$ in the new scatter plane. Then

$$\overline{\Psi} = 38.97G(t)^{0.0815}, \quad (5)$$

and the coefficient of determination is 0.5937.

In order to extract the predictive capability of equation (5) for the real-time jet power (that which is concurrent with the EUV measurements), $Q(t)$, consider the following. The EUV emission and the jet launching both originate in the immediate vicinity of the central supermassive black hole Punsly (2015). The fundamental assumption of this analysis is as follows. Since the EUV and the jet emanate from a common compact region, the correlation found in Fig. 2 between these powerful dynamic elements is not spurious or coincidental, but results from an actual physical connection between, $\alpha_{\rm EUV}(t)$, $L_{\rm bol}(t)$ and $Q(t)$ in real time. In particular, the average trend in Fig. 2 is a direct consequence of this real-time interaction, or alternatively stated equation (5) is a consequence of a more fundamental quasi-simultaneous relation

$$\log Q(t) = 38.97G(t)^{0.0815}. \quad (6)$$

However, this relationship can only be true in an average sense due to variations from RLQ to RLQ, and epoch to epoch variations in both the geometry as well as the physical state of the innermost accretion flow. Describe the stochastic behaviour of $\log(Q(t))$ by a probability distribution, $\Psi\{Q[G(t)]\}$, that represents the physics of a complicated dynamical system created by an ensemble of numerous microphysical domains. From equations (5) and (6), the mean of the distribution is, $\mu[\Psi\{Q[G(t)]\}] \equiv \overline{\Psi} = 38.97G^{0.0815}$, where G is the time average of $G(t)$. To estimate the variance of $\Psi\{Q[G(t)]\}$, note that each data point in Fig. 2 is a random time snapshot of the innermost accretion flow, so the best fit to the trend represents the time averaged configuration for a given $\log(\overline{Q})$ and the dispersion from this trend results from $G(t)$ (and therefore $Q(t)$ by equation 6) varying from the mean value. From the scatter in the $\log[\overline{Q}]$–$\log Q(t)$ plane, one can compute the standard deviation, $\sigma = 0.46$. Assuming a normal distribution, Z,

$$\Psi\{Q[G(t)]\} = Z[\mu = 38.97G^{0.0815},\ \sigma = 0.46]. \quad (7)$$

Table 1. Prominent emission lines properties from the SDSS spectrum.

Line	Broad component FWHM (km s^{-1})	Full line FWHM (km s^{-1})	Line shift (km s^{-1})	Redward asymmetry A	Absorption FWHM (km s^{-1})	Absorption velocity (km s^{-1})	Notes
Mg II	3060	4110	440	0.32	305/370[a]	−2632/−2609	1
C III	3702	4290	430	0	0	–	–
C IV	3070	3870	265	0.15/0.24[b]	1200	−2663	2

Notes. [a]The two absorption widths are from resolved doublet. [b]The larger asymmetry is from Anderson et al. (1987) as seen in Fig. 3.

Based on the confidence contours (computed from $\Psi\{Q[G(t)]\}$), plotted as dashed blue curves in the bottom frame of Fig. 2, $7.3 \times 10^{45}\,\mathrm{erg\,s^{-1}} < Q(t) < 4.8 \times 10^{47}\,\mathrm{erg\,s^{-1}}$ with 90 per cent confidence. A large $Q(t)$ is consistent with the existence of a powerful radio core $\approx 4.9 \times 10^{44}\,\mathrm{erg\,s^{-1}}$ (Garrington, Conway & Leahy 1991; Lonsdale, Barthel & Miley 1993; Akujor et al. 1994).

As a verification of the validity of this method consider, the outlier in Fig. 2, 3C 288.1. The EUV deficit is much less than expected for the value of $\overline{Q}$. However, the radio core is rather weak with a 1–100 GHz luminosity of $\approx 1.0 \times 10^{43}\,\mathrm{erg\,s^{-1}}$ (Reid et al. 1995). The source has very little intrinsic absorption as evidenced by the flat EUV spectral index, so one expects a direct line of sight to the core. This implies that it is an intrinsically weak radio core with no significant free–free absorption or Doppler de-boosting. The conclusion is that 3C 288.1 is an outlier in Fig. 2 because the quasar is currently in a state of relatively weak radio activity.

3 UV EMISSION LINES AND ABSORPTION LINES

One of the most striking trends in the quasar phenomenon is that the BAL prominence is anticorrelated with the radio loudness of the quasar (Becker et al. 2001; Shankar, Dai & Sivakoff 2008). If one considers RLQs with extended emission on supergalactic scales (radio lobes) this anticorrelation is stronger. Only a handful of BALQSO candidates with extended radio emission have ever been found even in deep surveys (Gregg, Becker & de Vries 2006). Considering the large jet power in 3C 270.1, the claim of Gibson et al. (2009) that there was a C IV BAL in the SDSS spectrum (under the formal definition of Weymann et al. 1991 per equation 8, below) is startling. Even more so because the absorption of C IV in 3C 270.1 was analysed by R. Weymann in Anderson et al. (1987) and was an example of what is not a BAL, but what they call associated absorption. Since the anticorrelation between the power of extended radio lobes and BALs is likely related to the phenomenon of jet launching and BAL wind formation, this controversial finding is examined in detail in this section. The top frame of Fig. 3 is an overlay of the MMT (Multiple Mirror telescope) data from Anderson et al. (1987) and the SDSS data (see also Table 1). The O VI absorption is displayed in the bottom frame of Fig. 3. The upper limit of the continuum is solid red (the fourth-order polynomial fit) and the blue dashed line is the power-law fit from Fig. 1. It is clearly broader and higher velocity than the C IV absorber. The data were plotted with a smoothing window of 1.25 Å in the quasar rest frame.

The BALnicity index, BI, was defined in Weymann et al. (1991) as

$$\mathrm{BI} = \int_{v=-25000}^{v=-3000} [1 - F(v)/0.9] C \, \mathrm{d}v, \tag{8}$$

where $F(v)$ is the flux density normalized to the continuum level as a function of v, the velocity from the QSO rest-frame line emission frequency in km s^{-1}. The step function, $C(v) \neq 0$ if and only if there more than 2000 km s^{-1} of continuous absorption beyond −3000 km s^{-1}. This measure of broad absorption has been borne out over the years as very robust. More lax measures of absorption (such as associated absorption and mini-BALs) have turned out to represent different classes of objects, that have less X-ray absorption than BALQSOs and larger radio luminosity than bona fide BALQSOs (Punsly 2006; Knigge et al. 2008; Shankar et al. 2008). In deriving this measure, the authors considered narrower associated absorption and decided that this was a different phenomenon. The function $C(v)$ was designed to segregate out this type of absorption.

In order to implement equation (8), we need an accurate determination of the redshift. From the [O III] narrow lines observed in Jackson & Rawlings (1997), we obtain $z = 1.5226$. This agrees with our UV line analysis of the SDSS data, 1.5228 ± 0.0013 at the 1σ confidence level. $C \neq 0$ requires absorption beyond −5000 km s^{-1}. Thus, from Fig. 3 and Table 1, there is no absorption beyond −5000 km s^{-1} and $C = 0$ for C IV and O VI for all v. These absorption have BI = 0 and are examples of associated absorption that is common in RLQs.

O VI shows absorption maxima at $v \approx -4290$, −2480 km s^{-1} and C IV shows absorption at $v \approx -2660$ km s^{-1}. From the data in Aldrcoft, Bechtold & Elvis (1994) and the SDSS data in Table 1, the narrow Mg II absorption arises from gas that has an outflow velocity of $v \approx -2620$ km s^{-1}. This indicates the following wind dynamic. There is a narrow absorption line wind with $v_{\mathrm{wind}} \approx 2600$ km s^{-1} and second high-ionization wind with $v_{\mathrm{wind}} \approx 4300$ km s^{-1}. It is not clear if the high-ionization wind is the base of a common wind that coasts at $v_{\mathrm{wind}} \approx 2600$ km s^{-1} farther out.

The UV emission lines were decomposed into a broad, a very broad and narrow components as has been previously documented in the analysis of eigenvector 1 and the Population A/B dichotomy used to classify quasar spectrum (Sulentic et al. 2007). It is demonstrated that the line profiles are typical of RLQ, Pop. B sources which are at the opposite end of eigenvector 1 from the BALQSOs (Pop. A sources). From Table 1, the peaks of the C IV, C III] and Mg II broad components show small redshifts relative to the quasar systemic velocity consistent with Pop. B sources (Sulentic et al. 2007). Secondly, here is a tendency for redward asymmetric profiles which is also associated with RLQ, Pop. B sources. Using the measure for asymmetry from Wills et al. (1995), A, that is defined in terms of the full width at half-maximum, FWHM, in Å; the mid-point of an imaginary line connecting a point defined at 1/4 of the peak flux density of the BEL on the red side of the BEL to 1/4 of the peak flux density on the blue side of the BEL, λ_{25}, and a similar mid-point defined at 8/10 of the flux density maximum, λ_{80}, as

$$A = \frac{\lambda_{25} - \lambda_{80}}{\mathrm{FWHM}}. \tag{9}$$

A positive value of A means that there is excess flux in the red broad wing of the emission line. The redward asymmetry, especially of C IV, has been previously associated with RLQs (Punsly 2010). The values in Table 1 are large even for RLQs. Finally, the small

intensity ratio Al III 1860/C III] 1909 ≈ 0.08 is typical of Pop. B sources (Bachev et al. 2004). The designation as a Pop. B source is consistent with the Mg II and C IV absorption widths in Table 1. The narrow widths are typical of narrow absorption lines not BALs.

Using the Mg II broad component width from Table 1, we obtain mass estimates for the central black hole $\log M_{\rm bh} = 8.89$ and $\log M_{\rm bh} = 8.99$ from the methods of Shen & Liu (2012) and Trakhtenbrot & Netzer (2012), respectively. Combining these estimates with $L_{\rm bol}$ from Section 2 indicates an Eddington rate, $L_{\rm bol} = 0.48 \pm 0.10 L_{\rm Edd}$. This is very high for a Pop. B source and is more typical of a Pop. A, radio quiet source. Thus, 3C 270.1 is extreme in all its properties, a very strong jet and a very luminous accretion disc.

4 CONCLUSION

In the second section, the EUV spectrum of 3C 270.1 was found to have $\alpha_{\rm EUV} = 2.98 \pm 0.15$. It was shown that 3C 270.1 has all the properties associated with the one of the most powerful RLQ jets in the known Universe. An argument was made that the $\log[\overline{Q}]$–$\alpha_{\rm EUV}$ scatter plane (Fig. 2) can be used to estimate a confidence interval for real-time jet power, $Q(t)$. Unlike other correlations in the literature involving $\overline{Q}$, such as with emission line properties as in Willott et al. (1999), it was noted that both the EUV and $Q(t)$ originate from near the central black hole and the correlation in the $\log[\overline{Q}/L_{\rm bol}]$–$\alpha_{\rm EUV}$ scatter plane therefore indicates a nearly simultaneous causal contact between the two dynamical processes. If not for this circumstance, the estimator for $Q(t)$ would be unjustified. The method developed here might have application to other extreme quasars in future studies. In the third section, it was shown that the C IV and O VI absorption had BI = 0. Thus, 3C 270.1 is not a BAL quasar as classically defined, but displays the well-known associated absorption that occurs in many RLQs.

The details of the correlation found in Fig. 2 was elucidated in two previous studies. First, a correlation induced by larger black hole masses and lower accretion rates in RLQs was ruled out empirically as a plausible explanation due to the indistinguishable SED peak in RLQs and RQQs (Punsly 2014). A partial correlation analysis in Punsly (2015) indicates that the fundamental physical correlation amongst quantities is between $Q/L_{\rm bol}$ and $\alpha_{\rm EUV}$. This correlation is not explained by the Laor & Davis (2014) disc wind. However, as discussed in Punsly (2014) the most likely explanation of the correlation, jets from magnetic flux in the inner accretion disc, can coexist with these winds. Consistent 3D MHD numerical models are those in which an annular region ($\sim$ 2–4 black hole radii wide) of the innermost accretion flow, adjacent to the black hole, is perforated by islands of large-scale poloidal (vertical) magnetic flux. The rotating flux distribution associated with the magnetic islands is the source of the relativistic jet and it also displaces the EUV emitting gas, thereby causing an EUV deficit that is correlated with $Q(t)$ (Punsly 2015). The degree of magnetization of the inner disc determines scaling relations for jet power and the EUV decrement. In particular, based on fig. 4 of Punsly (2015), the EUV deficit and jet power of 3C 270.1 indicates that $\approx$ 50 per cent of the innermost accretion flow is displaced by the magnetic islands.

ACKNOWLEDGEMENTS

BP benefited from affiliation ICRANet.

REFERENCES

Akujor C., Luedke E., Browne I. W. A., Leahy J. P., Garrington S. T., Jackson N., Thomasson P., 1994, A&AS, 105, 247
Aldrcoft T., Bechtold J., Elvis M., 1994, ApJS, 95, 1
Anderson S., Weymann R., Foltz C., Chaffee F., 1970, AJ, 94, 278
Bachev R., Marziani P., Sulentic J. W., Zamanov R., Calvani M., Dultzin-Hacyan D., 2004, ApJ, 617, 171
Becker R. et al., 2001, ApJS, 135, 227
Blundell K., Rawlings S., 2000, AJ, 119, 1111
Cardelli J., Clayton G., Mathis J., 1989, ApJ, 345, 245
Davis S., Laor A., 2011, ApJ, 728, 98
deVries W., Becker R., White R., 2006, AJ, 131, 666
Garrington S., Conway R., Leahy J., 1991, MNRAS, 250, 173
Gibson R. et al., 2009, ApJ, 692, 758
Gregg M., Becker R., de Vries W., 2006, ApJ, 641, 210
Jackson N., Rawlings S., 1997, MNRAS, 286, 241
Knigge C., Scaringi S., Goad M., Cottis C., 2008, MNRAS, 386, 1426
Laor A., Davis S., 2014, ApJ, 428, 3024
Lonsdale C., Barthel P., Miley G., 1993, ApJS, 87, 63
Punsly B., 2005, ApJ, 623, L9
Punsly B., 2006, ApJ, 647, 886
Punsly B., 2007, MNRAS, 374, L10
Punsly B., 2010, ApJ, 713, L232
Punsly B., 2014, ApJ, 797, L33
Punsly B., 2015, ApJ, 806, 47
Reid A., Shone D. L., Akujor C. E., Browne I. W. A., Murphy D. W., Pedelty J., Rudnick L., Walsh D., 1995, A&AS, 110, 213
Richards G. et al., 2011, AJ, 141, 167
Shankar F., Dai X., Sivakoff G., 2008, ApJ, 687, 859
Shen Y., Liu X., 2012, ApJ, 753, 125
Shull M., Stevans M., Danforth C., 2012, ApJ, 752, 162
Sulentic J. W., Bachev R., Marziani P., Negrete C. A., Dultzin D., 2007, ApJ, 666, 757
Trakhtenbrot B., Netzer H., 2012, MNRAS, 427, 3081
Weymann R. J., Morris S. L., Foltz C. B., Hewett P. C., 1991, ApJ, 373, 23
Willott C., Rawlings S., Blundell K., Lacy M., 1999, MNRAS, 309, 1017
Wills B. et al., 1995, ApJ, 437, 139
Zheng W., Kriss Gerard A., Telfer Randal C., Grimes John P., Davidsen Arthur F., 1997, ApJ, 475, 469

This paper has been typeset from a TEX/LATEX file prepared by the author.